Climate effects of a future net forestation scenario in CMIP6 models

Check for updates

James L. Gomez[1] ✉, Robert J. Allen[1], Larry W. Horowitz[2], Steven T. Turnock[3], Rosie A. Fisher[4], Olivia E. Clifton[5], Bryan K. Mignone[5], Elena Shevliakova[2] & Sergey Malyshev[2]

Forestation may reduce temperatures by lowering atmospheric CO_2. However, biogeophysical changes from forestation may weaken this cooling. We use twelve Coupled Model Intercomparison Project (CMIP6) models to quantify the biogeochemical (carbon cycle) and biogeophysical (non-carbon cycle) effects of net forestation, as quantified as the difference between the end of two future scenarios: ssp370-ssp126Lu and ssp370. Biogeochemical effects have an inferred global multi-model mean cooling (-0.08 ± 0.02 K). Changes in fires have no significant effect on land carbon storage globally. In contrast with studies indicating biogeophysical impacts counteract biogeochemical impacts by up to 50%, we find that biogeophysical effects lead to insignificant global mean cooling (-0.002 ± 0.041 K). Tropical land shows cooling (-0.058 ± 0.058 K) with eight of twelve models indicating cooling, consistent with prior studies. Using the Surface Energy Balance Decomposition, we find cooling is primarily from increased evapotranspiration and decreased downwelling solar radiation related to clouds and aerosols.

Afforestation, or the planting of trees in areas where there is no recent tree cover, and reforestation, or the planting of trees where they have been recently removed, have been proposed as a natural method of reducing CO_2 in the atmosphere[1-3]. Reforestation and afforestation (hereinafter, forestation) increase the carbon stored in the terrestrial biosphere[1,2] and thus reduce atmospheric CO_2. This CO_2 sequestration is referred to as a "biogeochemical effect." A previous study has indicated that forestation has a mitigation potential of 4.9 $GtCO_2$/year at 200 US $/tCO_2$ in 2050 through biogeochemical effects[2], which implies a role for forestation to help limit warming to below 2 °C relative to preindustrial times.

In addition to the effects on atmospheric CO_2, forestation can also affect temperature through biogeophysical effects. "Biogeophysical effects" are defined as changes in temperature due to changes in the physical properties of the land that influence the surface energy balance (i.e., non-carbon cycle effects). For example, this includes changes in surface albedo (α), evapotranspiration (ET), and natural emissions of trace gases, aerosols, and their precursors important for atmospheric composition. Biogeophysical effects are important[4], as previous modeling studies have indicated that up to 50% of biogeochemical effects may be offset by biogeophysical effects in various deforestation and forestation scenarios[5-9]. More research is needed on the drivers of differences across previous estimates, possibly due to model and scenario differences. Here, we examine whether there are robust responses in biogeophysical and biogeochemical effects across the current

generation of Earth System Models in a common future net forestation scenario, with the aim of advancing our understanding of how forestation may contribute to climate change mitigation.

In addition to the fact that biogeochemical vs. biogeophysical responses can be of different sign, there are both biogeophysical warming and cooling impacts, necessitating analysis frameworks of the biogeophysical responses that allow the identification of individual process drivers. First, we discuss agents of biogeophysical cooling. Relative to other land surface types, trees can cool the surface through high ET and therefore increased latent heat flux (LE)[5,10,11]. Increased ET and temperature decreases can also lead to increased humidity. Higher humidity can decrease downwelling surface shortwave radiation (SW_d) through increased cloud formation and direct atmospheric absorption of shortwave radiation (e.g., by water vapor)[12]. Furthermore, prior studies indicate that increases in leaf area index and particular tree species are associated with enhanced emissions of biogenic volatile organic compounds (BVOCs), which can be oxidized and form organic aerosols (OA). OA are highly reflective and can reduce SW_d and act as cloud condensation nuclei, having net surface cooling effects[6,13-16].

These biogeophysical cooling effects could be countered by the biogeophysical warming effects of forestation[17,18]. Trees decrease surface albedo through surface darkening[5,19] and may increase tropospheric ozone (O_3) and methane (both greenhouse gases)[5,6,15,16,20] through increased BVOC emissions. The formation of clouds from increased ET and aerosol

[1]Department of Earth and Planetary Sciences, University of California, Riverside, Riverside, CA, USA. [2]Geophysical Fluid Dynamics Laboratory, National Oceanic Atmospheric Administration, Princeton, NJ, USA. [3]Met Office, Exeter, Devon, UK. [4]Center for International Climate Research, Oslo, Norway. [5]ExxonMobil Technology and Engineering Company, Annandale, NJ, USA. ✉e-mail: jgome222@ucr.edu

concentration can also increase surface downwelling longwave flux (LW_d). Enhanced vegetation cover and decreased wind speed can also decrease dust aerosol emission, which scatters solar radiation[21–23]. Changes in wind speed from increases in surface roughness can also alter vertical mixing and, thus, sensible and latent fluxes, which can lead to local warming or cooling. Water vapor, aerosols, and sensible heat (H) can be transported via atmospheric circulation over long distances, creating a potential for remote biogeophysical effects[24]. A recent study indicates the potential for forestation to remotely affect climate through adjusted atmospheric and oceanic circulation[25]. They show that the remote climate effects of highly idealized forestation (i.e., grassland, cropland, shrubs, and urban areas are turned into forests, resulting in 80% forest coverage) are associated with a weakening and poleward shift of the northern mid-latitude circulation and a slowdown the Atlantic Meridional Overturning Circulation (AMOC).

To get a process-oriented view of the changes in temperature due to the biogeophysical effects of forestation, we employ the Surface Energy Balance Decomposition (SEBD), which allows us to attribute changes in temperature to changes in downwelling shortwave and longwave radiation, sensible and latent heat fluxes, and albedo (Methods). This method has been used in prior studies examining land cover changes[5]. Using the SEBD, mechanisms for the changes in temperature can be further discerned through cross-correlation analysis (e.g., if clouds or aerosols are responsible for a change in surface temperatures).

Observations can be useful in learning more about the impacts of forestation. Primarily, signals such as changes in ET or surface reflectivity can be discerned from observation-based studies. For example, ref. 19 analyzed forestation in China (as of 2008) and found significant daytime cooling associated with higher ET. Similarly, ref. 26 found that reforestation in the eastern United States slowed warming associated with climate change[26]. Performing new observational studies of forestation is expensive and time-consuming, as it takes decades for forestation to effectively store carbon, making studying the long-term and future effects of forestation difficult[1,17]. In addition, with observations alone, it is difficult to attribute causality concerning some effects of forestation, such as changes in aerosol concentration or cloud cover. Many of these issues can be circumvented with Earth System Model simulations, which are used here. Earth System Models allow quantification of local and remote effects[25], in addition to other impacts (e.g., changes in fires). In addition, climate models allow for studying global forestation, so the specific impacts of increased tree cover can be compared across latitudes, as prior studies indicate major differences in temperature responses depending on where a tree is planted[5,17,18]. Although model uncertainty exists, a multi-model analysis (as performed here) allows robust changes and driving mechanisms to be quantified globally.

Understanding the effects of forestation on wildfires is vital, as an increase in fire carbon emissions (fFire) could offset the increase in net primary production from forestation. For example, higher fuel load in temperate and boreal regions is associated with more frequent and severe fires[27–37]. Therefore, as trees contain more fuel than grasses or crops, forestation in the higher latitudes may lead to increased fFire. Alternatively, replacing tropical grasses with trees may reduce fire emissions. Most fires in the tropics occur in grasses, which have an annual life cycle that makes them more susceptible to fires than trees in the region[32]. Therefore, changing the type of vegetation itself can affect fires through changes in fuel type; therefore changes in fires are also connected to biogeophysical effects, as differences in regional relative humidity and temperature can significantly impact fuel flammability and availability[24,38–41]. In summary, the effects forestation on wildfire occurrence and severity depend on whether changes in flammability (from changes in fuel type or from biogeophysical effects) or differences in fuel load dominate the signal.

Specifically, our study quantifies how net forestation affects climate at the end of the 21st Century, using the difference between two Coupled Model Intercomparison Project Phase 6 (CMIP6) 21st-century experiments and 12 Earth System Models (Supplement Table S1). We examine the multi-model annual averages from 2070-2099. The experiments are: 1. ssp370, which features relatively significant increases in greenhouse gases and global mean deforestation as specified by the SSP3-7.0 scenario; and 2. ssp370-ssp126Lu, which is identical to ssp370 except it features land cover changes from the SSP1-2.6 scenario; SSP1-2.6 is characterized by global mean forestation and prevented deforestation (Supplement Figure S1)[42–45]. The difference between ssp370 and ssp370-ssp126Lu yields only the effects of land cover change (i.e., net forestation, since afforestation, reforestation, and avoided deforestation in ssp370-ssp126Lu greatly outweigh deforestation in ssp370). While all models simulate carbon sequestration in vegetation and soil, they use prescribed atmospheric CO_2, and therefore, carbon sequestration does not change atmospheric CO_2. Thus, we estimate the biogeochemical effect offline using the Transient Climate Response to Emissions (TCRE).

Figure 1 illustrates how forestation can affect temperature through biogeophysical and biogeochemical effects and serves as a road map for our study. The primary objectives of this study are to quantify the net
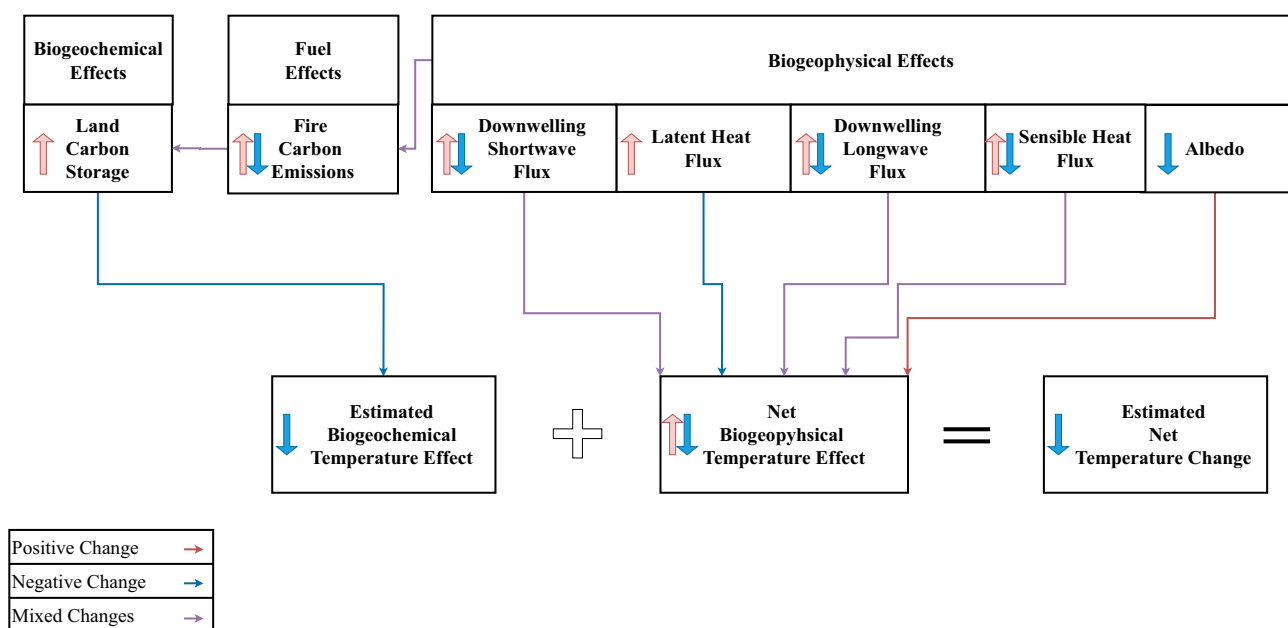

Fig. 1 | Flowchart for possible global changes in biogeophysical and biogeochemical effects of forestation. Red lines represent net positive changes, blue lines represent net negative changes, and purple lines represent uncertain effects. Colors are based on expected changes per prior literature cited in the introduction.

biogeophysical effect on temperature (as well as the contributions of the individual components of the surface energy budget via SEBD), to quantify how biogeophysical changes alter *fFire* and how this influences the biogeochemical effect, and to quantify the biogeochemical effect on temperature. Expected responses to forestation, as suggested by previous literature, are highlighted, with notable uncertainty in the sign of the response for *fFire*, downwelling shortwave radiation (SW_d), H, and LW_d.

Results

Changes in Land Cover under Net Forestation

Figure 2 shows the multi-model annual mean change over the last 30 years (2070–2099) in tree fraction (Fig. 2a), grass fraction (Fig. 2b), and crop fraction (Fig. 2c) in ssp370-ssp126Lu compared to ssp370. The supplement includes individual models' differences (Supplement Figs. S2–S4). Figure 2 shows that the difference between ssp370-ssp126Lu and ssp370 yields a
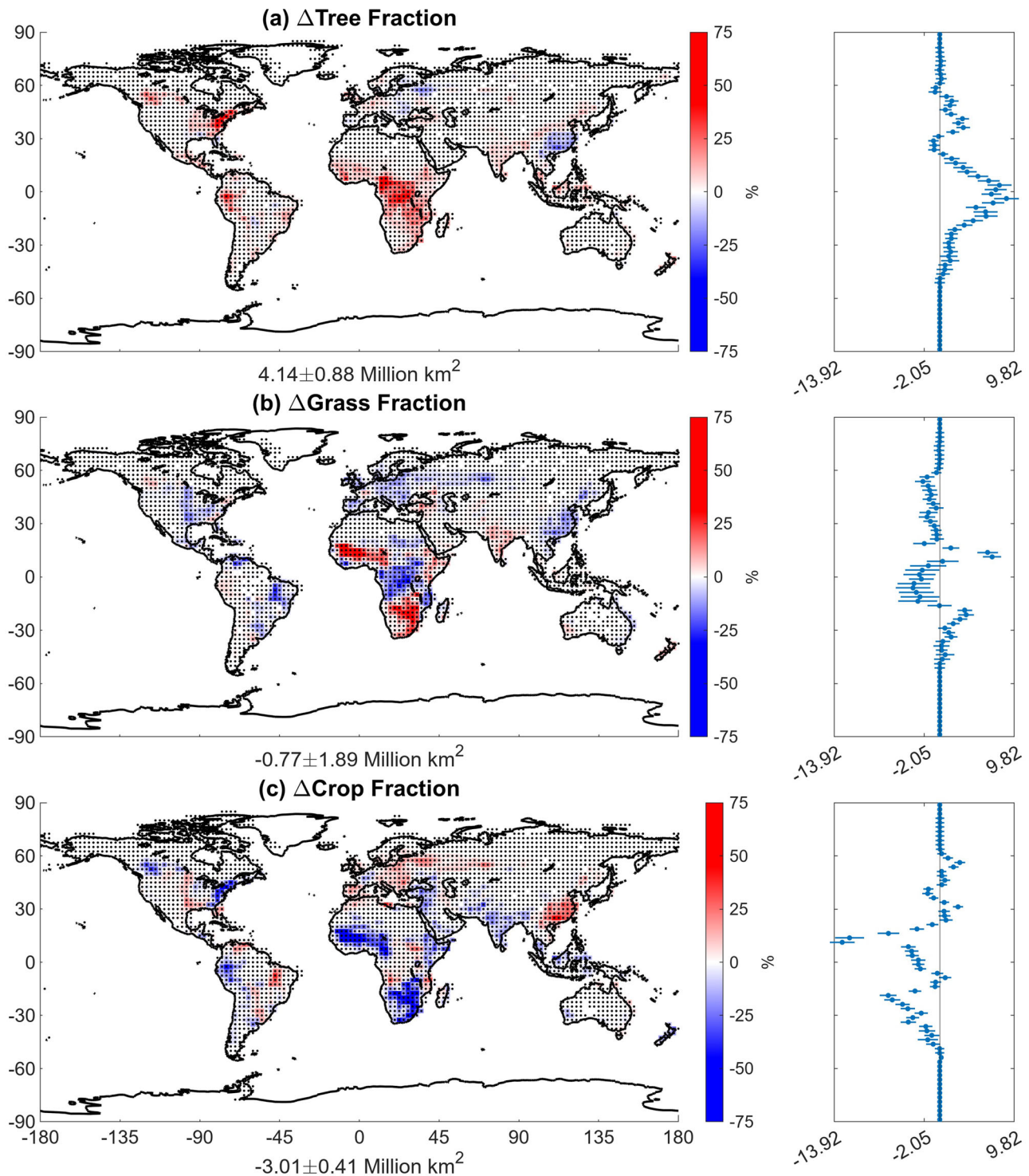
Fig. 2 | Multi-model mean land cover change between ssp370-ssp126Lu and ssp370 over years 2070-2099 for 12 climate models. Multi-model mean differences in (**a**) tree fraction, (**b**) grass fraction, and (**c**) crop fraction. Units are %. The global mean change (in million km²) and uncertainty are indicated underneath each panel. Black dots represent statistically significant changes at the 95% confidence interval using a two-tailed test. Depicted to the right of each map is a zonal mean of each value, with the uncertainty based on the 95% confidence interval of the model spread.

substantial increase in trees globally (i.e., net forestation). Hereinafter, we refer to the difference between the scenarios as "net forestation." The increase in tree fraction globally is generally in place of crops, followed by grass.

Overall, there is a 4.14 ± 0.88 million km^2 increase in tree area cover under net forestation (about half the area of the contiguous United States). Uncertainty here and in the text throughout the manuscript is based on the 95% confidence interval across the models, estimated as $1.96 \times$ standard error (Methods). These errors, therefore, quantify the differences between the models. Crop fraction decreases at -3.01 ± 0.41 million km^2, followed by a (nonsignificant) decrease in grass fraction at -0.77 ± 1.89 million km^2. The uncertainty in the fractional land cover changes results from differences among the individual models (Supplement Figs. S2–S4) and how they implement the common harmonized land use drivers[46]. In particular, considerable uncertainty in the change in grass fraction results from the models with dynamic vegetation (i.e., changes in vegetation type are explicitly simulated). In dynamic vegetation models, the model projects the type of vegetation (i.e., shrubs vs. grasses vs. trees, as opposed to this being prescribed as forest in models with static vegetation) on the unmanaged land converted from managed land. This applies to GFDL-ESM4, UKESM1-0-LL, and MPI-ESM1-2-LR, all of which have a more considerable grass increase, at the expense of forest cover, than the static vegetation models (Supplement Fig. S2 & S3, Supplement Table S2).

The highest increases in tree fraction are on the east coast of the United States, in central Africa, and in northern South America. Overall, the change in tree fraction is dominated by the tropics, particularly by the Congo. The scenarios ssp370 and ssp126 are determined by different IAMs and are based on different socioeconomic assumptions, climate targets, and policy assumptions (such as planting more bioenergy crops). While there are substantial decreases in forest area in ssp370 and increases in forestation and avoided deforestation in ssp126[42,47], forestation does not occur everywhere in the difference between them. For example, Fig. 2a demonstrates deforestation in China in ssp370-ssp126Lu relative to ssp370. This deforestation is associated with increased crop fraction (Fig. 2c). It is also important to note that while grass fraction decreases globally, it increases significantly in the Sahel and South Africa (Fig. 2b). Changes in shrub fraction are much smaller than other land fraction changes and are mostly regionally constrained to southern Africa (Supplement Fig. S5). Also of note are increases in bare soil fraction in the Sahara desert that correspond to decreases in crop fraction (Supplement Figs. S1, S4, & S6).

Biogeophysical impacts on regional climate

First, we examine the 2070–2099 biogeophysical impacts of net forestation on near-surface air temperature (T_{as}). There is insignificant global cooling of -0.002 ± 0.04 K and insignificant global land-only cooling of -0.01 ± 0.05 K. However, there are substantial model differences at the global scale; four of the 12 models yield significant global mean warming, and five of the 12 models yield significant global mean cooling (Table 1; Supplement Fig. S7). Similarly, four models yield significant land-only warming, whereas four yield significant land-only cooling.

Despite model differences globally, the models agree more on changes in the tropics, where most of the cooling over land occurs. For example, over land in the tropics ($-15°$ to $+15°$ latitude), there is a significant multi-model change of -0.058 ± 0.058 K, with 8/12 models agreeing that there is regional mean cooling there (though only five have significant cooling). Over land in the northern hemisphere (latitude > 15°), there is insignificant warming of 0.035 ± 0.079 K (six of twelve models agree on warming). There are, however, areas of significant warming in the northern hemisphere. For example, central/western Canada and, to some extent, central Europe (Fig. 2a) feature relatively large forestation and significant increases in T_{as} (Fig. 3a). At lower latitudes of the northern hemisphere, China shows significant increases in T_{as} associated with deforestation.

Figure 3 shows the global and latitudinal distributions of the biogeophysical effects of net forestation on T_{as} (Fig. 3a, b), ET (Fig. 3c, d), and α (Fig. 3e, f). Associated with significant decreases in T_{as} in the tropics (Fig. 3a)

Table 1 | 2070–2099 changes in near-surface air temperature due to the biogeophysical effects of net forestation in the northern hemisphere (NH; latitudes ≥ 15°N), southern hemisphere (SH; latitudes ≤ 15°S), the tropics (TR; latitudes between 15°S and 15°N) and globally for all 12 models

ΔT_as (K)	Global T_as	NH T_as	SH T_as	TR T_as	Global T_as (Land)	NH T_as (Land)	SH T_as (Land)	TR T_as (Land)
ACCESS-ESM-5	0.0033 ± 0.006	0.0044 ± 0.0089	−0.0061 ± 0.0079	0.015 ± 0.013	0.015 ± 0.0063	0.0019 ± 0.016	−0.0071 ± 0.019	0.058 ± 0.022
BCC-CSM2-MR	−0.14 ± 0.015	−0.14 ± 0.033	−0.18 ± 0.018	−0.093 ± 0.019	−0.15 ± 0.017	−0.17 ± 0.063	−0.16 ± 0.053	−0.1 ± 0.035
CanESM5	−0.0036 ± 0.021	0.0066 ± 0.032	−0.037 ± 0.023	0.028 ± 0.04	0.016 ± 0.023	0.016 ± 0.059	0.025 ± 0.061	0.0058 ± 0.073
CESM2	0.058 ± 0.011	0.18 ± 0.018	0.012 ± 0.012	−0.052 ± 0.023	0.0074 ± 0.013	0.18 ± 0.033	−0.034 ± 0.033	−0.17 ± 0.037
CMCC-ESM2	0.14 ± 0.027	0.3 ± 0.027	0.04 ± 0.021	0.068 ± 0.055	0.18 ± 0.028	0.35 ± 0.073	0.097 ± 0.065	0.041 ± 0.07
CNRM-ESM2-1	0.063 ± 0.021	0.14 ± 0.033	0.019 ± 0.025	0.011 ± 0.037	0.07 ± 0.022	0.099 ± 0.059	0.11 ± 0.063	−0.028 ± 0.064
GFDL-ESM4	−0.037 ± 0.027	−0.095 ± 0.039	0.0088 ± 0.026	−0.019 ± 0.052	−0.04 ± 0.023	−0.11 ± 0.067	0.026 ± 0.059	−0.023 ± 0.061
IPSL-CM6A-LR	−0.077 ± 0.022	−0.095 ± 0.029	−0.049 ± 0.025	−0.092 ± 0.047	−0.11 ± 0.023	−0.056 ± 0.05	−0.042 ± 0.069	−0.25 ± 0.071
MIROC-ES2L	−0.027 ± 0.019	−0.043 ± 0.029	−0.0046 ± 0.015	−0.036 ± 0.037	−0.068 ± 0.02	−0.034 ± 0.054	−0.066 ± 0.055	−0.11 ± 0.057
MPI-ESM1-2-LR	−0.024 ± 0.023	−0.028 ± 0.033	−0.071 ± 0.019	0.044 ± 0.048	−0.021 ± 0.022	−0.017 ± 0.056	−0.033 ± 0.058	−0.01 ± 0.069
NorESM2-LM	0.0042 ± 0.034	0.11 ± 0.042	−0.038 ± 0.024	−0.082 ± 0.07	−0.026 ± 0.031	0.13 ± 0.07	−0.075 ± 0.061	−0.18 ± 0.092
UKESM1-0-LL	0.014 ± 0.007	0.005 ± 0.014	0.017 ± 0.0082	0.023 ± 0.013	0.042 ± 0.0079	0.022 ± 0.027	0.037 ± 0.024	0.072 ± 0.024
Mean	−0.0018 ± 0.041	0.029 ± 0.074	−0.023 ± 0.033	−0.015 ± 0.031	−0.0066 ± 0.048	0.035 ± 0.079	0.0093 ± 0.043	−0.058 ± 0.058

Values are given for land and ocean, as well as land only. Units are K. Individual model uncertainties are based on the 95% confidence interval of each model's 2070–2099 difference time series (i.e., ssp370-ssp126Lu − ssp370), while the uncertainty for the multi-model mean is based on the 95% confidence interval associated with the standard error of the signal across models. Bolded values are significant.
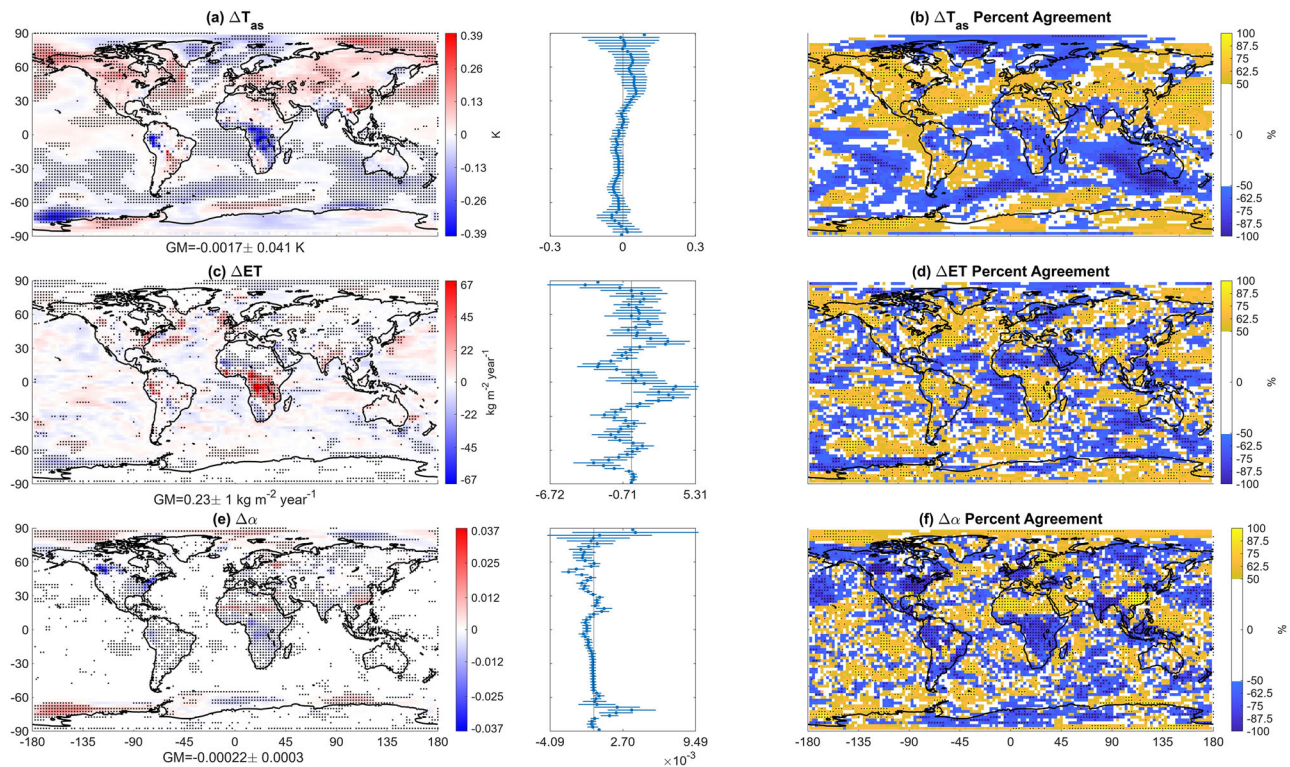
Fig. 3 | Biogeophysical effects of net forestation (ssp370-ssp126Lu − ssp370) over years 2070–2099. Multi-model annual mean response of (**a**) near-surface air temperature (T_{as}; K), (**c**) surface evapotranspiration (ET; kg m^{-2} year^{-1}), and (**e**) surface albedo (α; dimensionless). Black dots on (**a**), (**c**), and (**e**) symbolize statistically significant differences at the 95% confidence interval using a two-tailed test. The global mean change and its uncertainty are indicated underneath each panel. Depicted to the right of each multi-model mean map is a zonal mean of each variable, with the uncertainty based on the 95% confidence interval of the model spread. These plots share the same units as the color bar of the corresponding panel. Also shown are model percent agreement plots (%) for (**b**) T_{as}, (**d**) ET, and (**f**) α. Yellow colors indicate that the majority of the models yield a positive difference. In contrast, blue colors indicate that the majority of the models yield a negative difference. Black dots on (**b**), (**d**), and (**f**) show grid cells with at least 66% model agreement on the sign of the difference.

are significant increases in ET (Fig. 3c). These increases in ET in regions with increased tree fraction are associated with significant increases in near-surface relative humidity, cloud cover, and water vapor path (Q) (Supplement Fig. S8). This indicates that the increased ET associated with forestation significantly increases moisture flux into the atmosphere. However, while this change in relative humidity is associated with more clouds over regions with forestation, the precipitation response is more uncertain, with significant increases largely isolated to central Africa. Some regional changes in ET and α are robust between models (e.g., central Africa), with at least two-thirds of the models agreeing on the sign of the differences (symbols in Fig. 3d, f). There is less model agreement in changes in T_{as} (Fig. 3b), indicating relatively large inter-model diversity in the temperature response over regions with forestation. One place where there is a clear change in T_{as} as well as ET is in the tropics; in particular, central Africa and northeastern South America have significant changes in both quantities.

The spatial correspondence between tropical decreases in the multi-model average T_{as} and increases in ET suggests that changes in moisture flux due to an increased tree fraction have a cooling effect on the surface in many ESMs. Furthermore, in some regions (e.g., North America and central Europe), significant decreases in α in areas with forestation (Fig. 2a, Fig. 3e, f) correspond to significant warming. In the next section, we utilize the surface energy balance decomposition method to further explore how changes in ET and α, in addition to incoming shortwave and longwave radiation, impact surface temperatures.
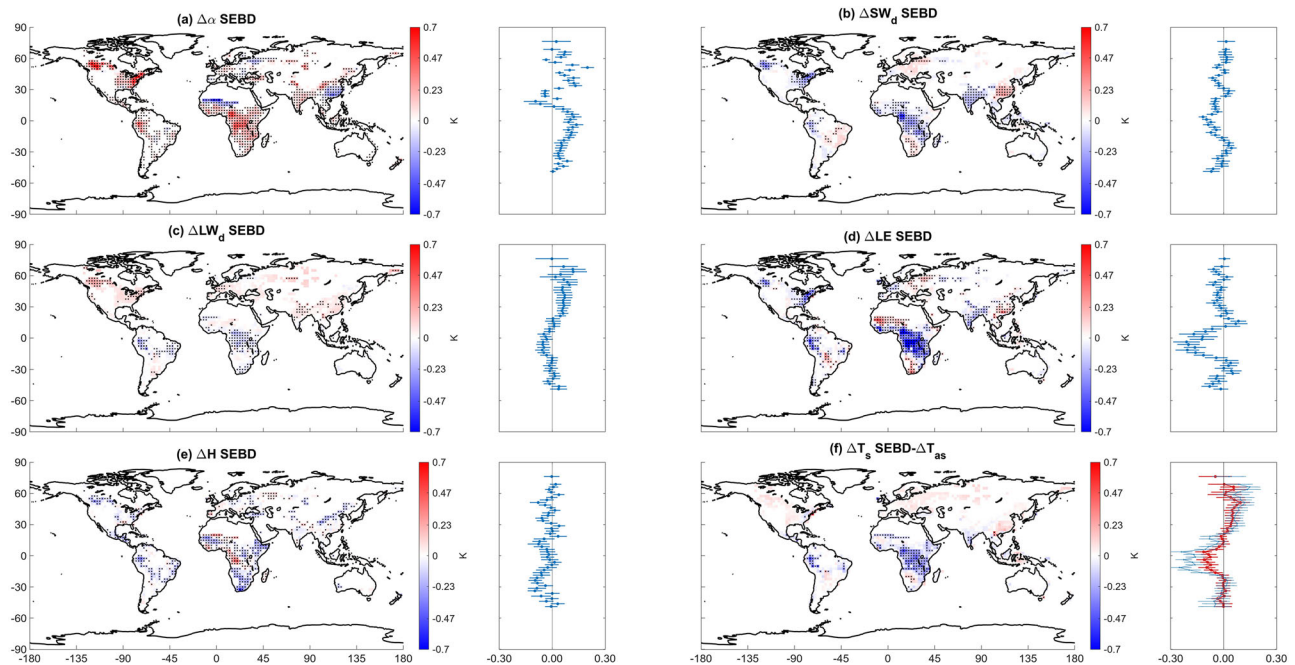
Surface energy balance decomposition

The surface energy balance decomposition (SEBD) relates changes in surface temperature (T_s) to changes in surface energy fluxes (Methods)[5]. To

better isolate the drivers of the 2070-2099 T_s response due to the land cover change, we apply the SEBD over grid cells with an increase or decrease in tree fraction greater than or equal to 1%[5] (hereinafter, sub-sampling). Figure 4 shows the multi-model mean SEBD.

We first note that the SEBD estimate of ΔT_s is generally not significantly different from the actual simulated ΔT_s (Supplement Fig. S9). However, prior work indicates that using T_s to approximate T_{as} results in overestimation of the temperature response associated with forestation[48,49]. We compare the SEBD estimate of ΔT_s to the simulated ΔT_{as} and find that the former is generally not significantly different from the latter, except near the equator where the SEBD overestimates cooling (Fig. 4f). For example, outside the tropics, the error bars overlap in the zonal mean, and there are no grid cells with significant differences (as indicated by a lack of symbols on the spatial map in Fig. 4f). We also note that the zonal mean T_s changes in Fig. 4f (subsampled to grid boxes where the tree fraction increases or decreases by at least 1%) are, in general, similar to those in Fig. 3a (zonal means over all longitudes). This includes tropical cooling and extratropical warming in the northern hemisphere. These signals (e.g., tropical cooling) are generally larger when sub-sampling, implying the importance of local (as opposed to remote) biogeophysical effects associated with trees. Southern hemisphere extratropical cooling, however, is more evident in Fig. 3a (e.g., over the oceans), implying the importance of remote effects (e.g., atmospheric or oceanic circulation changes).

In the tropics and northern hemisphere, the increases in tree fraction (Fig. 2a) coincide with a decrease in surface α (Fig. 3e), contributing to a positive change in T_s from α there (Fig. 4a). The decreases in surface SW_d (Supplement Fig. S10) and strong increases in LE (Supplement Fig. S11) counteract the α-driven increases in T_s near the tropics, leading to a net

Fig. 4 | Multi-model mean surface energy balance decomposition (SEBD) of the surface temperature (T_s) response under net forestation (ssp370-ssp126Lu − ssp370) over years 2070–2099 where tree fraction increases or decreases by at least 1%. SEBD estimated contributions of surface (**a**) albedo (α), (**b**) downwelling shortwave radiative flux (SW_d), (**c**) downwelling longwave (LW_d) radiative flux, (**d**) latent heat flux (LE), and (**e**) sensible heat flux (H). Panel (**f**) shows the corresponding SEBD estimated multi-model mean T_s response (i.e., the sum of individual component) minus the actual T_{as} response. Black dots on spatial maps symbolize statistically significant differences at the 95% confidence interval using a two-tailed test. Depicted to the right of each map is a zonal mean of each variable, with the uncertainty based on the 95% confidence interval of the model spread. The zonal mean plot for panel (**f**) shows the SEBD-estimated multi-model mean T_s (blue) and the actual T_{as} (red). Units are K.

cooling effect at the surface (Fig. 4b, d respectively). The LE effect on tropical T_s from increased ET is large, creating cooling effects of more than −0.7 °C) in some tropical areas.

In the northern hemisphere poleward of 15°N, the warming is primarily associated with the α SEBD term and secondly with the LW_d SEBD term, which overwhelm smaller changes in the LE, SW_d, and H SEBD terms. Therefore, forestation's surface darkening warming effect is a robust and significant signal among the models. Previous studies using the SEBD point to changes in LW_d being driven by the Planck feedback, where a warmer surface (e.g., due to surface darkening) emits more longwave radiation upwards, some of which is subsequently re-radiated back down to the surface via the atmospheric greenhouse effect (similarly, a colder surface is associated with lower LW_d, as seen in the tropics in Fig. 4c)[5,50].

To better understand the drivers of LW_d SEBD, we calculate its clear-sky ($LW_{d,cs}$) and cloud-only (all-sky minus clear sky; $LW_{d,cl}$) components (Supplement Fig. S12). Performing a cross-correlation analysis across grid cells, we find that the LW_d SEBD changes most significantly correlate with $LW_{d,cs}$ SEBD (r = 0.91; Table 2). We also find a relatively large and significant correlation between T_s and $LW_{d,cs}$ SEBD (r = 0.89; Table 2). Despite significant increases in clouds in many areas with forestation (Supplement Fig. S8g), clouds appear less important for explaining changes in LW_d SEBD. For example, the correlation between the LW_d SEBD and $LW_{d,cl}$ SEBD is insignificant (r = 0.002), and $LW_{d,cl}$ SEBD changes are generally opposite LW_d SEBD. This is particularly prominent over central Africa where the $LW_{d,cl}$ SEBD shows significant warming (Supplement Fig. S12b), consistent with an increase in cloud fraction (Supplement Fig. 8g), but in contrast to the cooling under LW_d and $LW_{d,cs}$ SEBD. The strong clear-sky LW_d SEBD and T_s correlation adds additional evidence that the Planck feedback drives the LW_d signal (i.e., some of the enhanced upwards long wave flux associated with surface warming is redirected back down to the surface under clear-sky conditions).

Significant decreases in SW_d contribute to significant cooling in the tropics (Fig. 4b), which is related to higher regional aerosol concentrations and enhanced cloud cover (Supplement Fig. S8g). To try to understand the importance of aerosol direct effects (e.g., scattering and absorption of solar radiation), we analyze the multi-model mean changes in clear-sky downwelling shortwave surface flux ($SW_{d,cs}$) SEBD. There is reduced $SW_{d,cs}$ SEBD in the tropics, with significant zonal mean cooling from about 10°S to 20°N (Supplement Fig. S13a). This decrease in $SW_{d,cs}$ SEBD contributes to the total cooling associated with the SW_d decrease (Supplement Fig. S13a). Correlating the multi-model mean change in $SW_{d,cs}$ SEBD with aerosol optical depth (AOD) for the seven models with AOD diagnostics available results in a significant correlation coefficient of r = − 0.66 (Table 3; see also Supplement Fig. S14). Note that the corresponding correlation between $SW_{d,cs}$ SEBD and Q is weak and nonsignificant at r = −0.09, implying aerosols, as opposed to water vapor, are important. Three of the 12 analyzed models (NorESM2-LM, UKESM1-0-LL, and GFDL-ESM4) have interactive BVOC emissions (Supplement Table S2). Two of the three models (NorESM2-LM and UKESM1-0-LL) show significant increases in BVOC emissions and OA, largely in the tropics (Supplement Fig. S15; Supplement Section 1). Also seen in some models (e.g., ACCESS-ESM1-5, GFDL-ESM4, CNRM-ESM2-1) is an increase in AOD over the Sahara desert and sub-Sahara (Supplement Fig. S16). For these models, there is a corresponding decrease in crop fraction and an increase in bare soil fraction (Supplement Figs. S16, S17, S2, & S6). Such changes, which occur around 10–20°N where the maximum $SW_{d,cs}$ decrease occurs (Supplement Fig. S14), might be the result of an increase in dust emissions (diagnostics of which these models did not archive).

Cloud changes are also important to SW_d. The cloud-only (all-sky minus clear-sky) downwelling surface shortwave radiation ($SW_{d,cl}$) SEBD term shows significant cooling in many afforested regions, including in the tropics (e.g., central Africa; Supplement Fig. S13b). This $SW_{d,cl}$ SEBD cooling corresponds spatially with a significant increase in cloud fraction

Table 2 | Grid cell-by-grid cell cross-correlations between LW_d SEBD (over grid cells with 1% change in tree fraction or more), its components, and variable responses

LW_d SEBD	1	0.91	−0.0015	0.26	0.72	−0.017
$LW_{d,cs}$ SEBD	0.91	1	−0.42	0.071	0.9	−0.37
$LW_{d,cl}$ SEBD	−0.0015	−0.42	1	0.39	−0.57	0.83
Q	0.26	0.071	0.39	1	−0.22	0.63
T_s	0.72	0.9	−0.57	−0.22	1	-0.53
CF	−0.017	−0.37	0.83	0.63	-0.53	1
	LW_d SEBD	$LW_{d,cs}$ SEBD	$LW_{d,cl}$ SEBD	Q	T_s	CF

Variables include the clear-sky and cloud-only components of LW_d ($LW_{d,cs}$ & $LW_{d,cl}$ respectively), water vapor path (Q), surface temperature (T_s), and cloud fraction (CF). Bolded values are significant at the 90% confidence interval. Correlations are based on years 2070-2099.

Table 3 | Grid cell-by-grid cell cross-correlations between SW_d SEBD (over grid cells with 1% change in tree fraction or more), its components, and variable responses

SW_d SEBD	1	0.58	0.93	−0.52	0.58	−0.81	−0.19
$SW_{d,cs}$ SEBD	0.58	1	0.23	-0.091	0.34	−0.19	−0.66
$SW_{d,cl}$ SEBD	0.93	0.23	1	−0.58	0.54	-0.88	0.053
Q	−0.52	−0.091	−0.58	1	−0.22	0.63	−0.34
T_s	0.58	0.34	0.54	−0.22	1	-0.53	-0.2
CF	−0.81	−0.19	−0.88	0.63	−0.53	1	−0.24
AOD	−0.19	−0.66	0.053	−0.34	-0.2	−0.24	1
	SW_d SEBD	$SW_{d,cs}$ SEBD	$SW_{d,cl}$ SEBD	Q	T_s	CF	AOD

Variables include the clear-sky and cloud-only components of SW_d ($SW_{d,cs}$ & $SW_{d,cl}$ respectively), water vapor path (Q), surface temperature (T_s), cloud fraction (CF), and aerosol optical depth (AOD). Cross-correlations that involve AOD only include models with AOD data available (see Supplement Fig. S14). Bolded values are significant at the 90% confidence interval. Correlations are based on years 2070–2099.

(Supplement Fig. S8g). Alternatively, there is also a significant decrease in cloud fraction over deforested areas in the northern hemisphere (Supplement Fig. S8g), which is associated with a significant increase in $SW_{d,cl}$ SEBD (Supplement Fig.S13b). As mentioned above, these changes in cloud fraction correspond to similar signed and significant changes in Q (Supplement Fig. S8a; $r = 0.63$ from Table 3), surface relative humidity (Supplement Fig. S8c), and ET (Fig. 3c) in many regions, implying the importance of trees to the atmospheric moisture flux. Furthermore, the T_s response to forestation may also contribute to the cloud response ($r = −0.53$; Table 3) through altered relative humidity, i.e., forestation both cools and adds atmospheric moisture, both of which act to increase relative humidity (and potentially clouds).

Thus, clouds and aerosols contribute to the significant surface cooling associated with changes in SW_d. Although $SW_{d,cs}$ SEBD yields stronger and more significant zonal mean tropical cooling (Supplement Fig. S13a) than does $SW_{d,cl}$ SEBD (Supplement Fig. 12b), there is better spatial agreement between SW_d and $SW_{d,cl}$ SEBD terms ($r = 0.93$; Table 3) than there is between SW_d and $SW_{d,cs}$ SEBD terms ($r = 0.58$; Table 3). Furthermore, $SW_{d,cl}$ tends to be larger in magnitude than $SW_{d,cs}$ in most regions. We also note that aerosols could impact the clouds, but we cannot quantify the aerosol-cloud effect here (e.g., due to a lack of relevant diagnostics).

H SEBD is also associated with significant changes in many regions with forestation, but these tend to be weaker in magnitude than the other SEBD components. Generally, the response in H is consistent with the expectation that forestation is associated with sensible heat-driven cooling. As trees increase surface roughness, they also increase vertical mixing[5], which transports heat away from the surface. However, there are some regional inconsistencies, including, for example, significant warming associated with ΔH in part of central Africa (Fig. 4e, Supplement Fig. S11c), where heavy forestation occurs (Fig. 2a).

We reiterate that there are substantial inter-model differences in their T_{as} responses to net forestation (i.e., half of the models yield global mean land cooling, whereas the other half yield the opposite; Table 1). To investigate further, we conduct the SEBD on two model subsets: the "warm" versus "cold" models, i.e., the models that yield global land-only warming versus those that yield cooling, respectively (each with six models). A smaller LE cooling effect in the tropics leads to larger tropical land-only warming in the warm model subset relative to the cold model subset (Supplement Fig. S18). Furthermore, across all models, there is generally a significant positive inter-model correlation between T_{as} and the LE SEBD over the tropics (Supplement Fig. S19d). This implies that models with higher LE in the tropics have more cooling over tropical land.

In the NH poleward of about 30°N, a larger α-driven warming effect leads to more warming over NH land in the warm model subset relative to the cold model subset (Supplement Fig. S18). This point is further supported by significant positive inter-model correlations between the α SEBD and T_{as} over much of the northern hemisphere (Supplement Fig. S19a). Additionally, the warmer models have a stronger increase in LW_d SEBD, presumably due to the larger α-driven NH warming leading to larger LW_d-driven warming, consistent with the Planck Feedback. Overall, most of the enhanced warming in the warm model subset relative to the cold model subset occurs in the NH extratropics, implying that model differences in the representation of the forestation effect on α contribute to the relatively large inter-model differences in the T_s response. Inter-model differences in their climate sensitivity may also contribute, as the correlation between each model's global land T_{as} response and their Equilibrium Climate Sensitivity (ECS; as obtained from ref. 51) is $r = 0.76$ (CMCC-ESM2 not included).

Remote effects

There are signs that net forestation in the experiments analyzed here yields remote climate effects. Although a majority of areas with significant changes in T_{as} over land (Fig. 3a) coincide with grid cells with a 1% change in tree fraction or higher (Fig. 2a), there are also significant temperature changes over parts of the ocean. In the northern hemisphere, for example, there is significant warming of much of the ocean (aside from the subpolar North Atlantic). In the southern hemisphere, there are regions of significant

cooling over the ocean. This difference in the sign of the oceanic response between hemispheres is consistent with the sign in response of T_{as} over land in each hemisphere (Fig. 3a, Table 1), which implies significant remote effects through changes in oceanic or atmospheric circulation. This hypothesis is supported by a lack of significant change in clouds in these areas of significant oceanic warming/cooling (Supplement Fig. S8). Furthermore, there are signs consistent with a weakening AMOC as indicated by a significant reduction in T_{as} in the subpolar North Atlantic (Fig. 3a), which is consistent with ref. 25. However, we also note that these effects may be due to internal climate variability rather than forced. Although we use 12 models, many of these models only performed one realization of ssp370-ssp126Lu. It is clear that there is large internal climate variability in individual model results, especially those with one realization (e.g., Supplement Fig. S8). Ideally, future studies should perform multiple realizations to improve signal-to-noise ratios and thus enable a more robust estimate of the remote effects of tree forestation.

Estimation of the Biogeochemical Effect

Forestation aims to sequester carbon within the land to reduce global atmospheric CO_2 concentrations. Figure 5a shows the multi-model mean change in carbon storage within the land (cLand) under net forestation over the years 2070-2099. Overall, there is a global mean increase in stored land carbon of 0.27 ± 0.13 kg m^{-2}. This corresponds to a global mean annual reduction in CO_2 of approximately 0.99 GtCO$_2$year^{-1}. 89% of this carbon is stored within the vegetation (cVeg; Fig. 5c), with robust model agreement that there is an increase. 7% of the increase is due to carbon stored within litter (cLitter), and the remaining 4% of the carbon is stored in the soil (cSoil) (Supplement Fig. S20). The most significant increases in cLand are in the areas with forestation in the tropics and the eastern United States. These increases also have robust agreement on the sign of the change across the models (Fig. 5c), with near-100% model agreement.

Using the transient climate response to cumulative carbon emissions (TCRE; Methods)[5], the multi-model mean biogeochemical effect on T_{as} is estimated as -0.08 ± 0.02 K over years 2070–2099. The estimated ΔT_{as} for each model can be found in Supplement Table S3. Overall, this 2070–2099 biogeochemical cooling is significantly larger than the global biogeophysical effect (-0.002 ± 0.041 K) and even the global land-only biogeophysical effect (-0.01 ± 0.05 K), which are both insignificant changes.

If we assume the global mean biogeochemical cooling can be applied to each grid box (under the assumption CO_2 is well-mixed), most regions yield a significant decrease in total (biogeochemical plus biogeophysical) T_{as} (Fig. 6a). Insignificant multi-model mean changes occur in much of western North America and northern Eurasia. The model agreement on the sign of the total ΔT_{as} (Fig. 6b) also shows robust cooling (more than 2/3 model agreement) throughout the tropics and southern hemisphere.

Fire

We will now quantify the effects of net forestation and its biogeophysical effects on fFire and the corresponding influence on the biogeochemical effect estimated in Section "Estimation of the Biogeochemical Effect." We note that only five models with the available data used an interactive fire module (Supplement Table S2). Of those models, three use some variation of the Community Land Model and its fire module[52,53]. Nonetheless, the five models are used to discern the fire response under net forestation and to determine if it significantly affects net primary production (npp) and cLand.

Figure 7a depicts the multi-model mean annual mean difference between ssp370-ssp126Lu and ssp370 (i.e., net forestation) of fFire for the five models with fire modules. Net forestation results in an insignificant global mean increase in fFire, with the largest increases in the Sahel and southern Africa. There are also significant increases in areas with forestation, such as Western Canada, India, and Central America. On the other hand, in tropical forests, there are decreases in fFire (Fig. 7a). The effect on fFire in these low-latitude regions is generally significant and generally has at least 2/3 model agreement on the sign of the response (Fig. 7b). Globally, the percent change in fFire is $+0.12 \pm 4.2$% (Supplement Fig. S21).

The insignificant global mean increase in fFire only weakly offsets the carbon sequestration benefit of forestation. In the five models, the global mean increase in fFire represents 13.1 ± 13.1% of the corresponding increase in npp (Supplement Fig. S21b). This supports the assertion that forestation does not significantly negatively impact the ability of the biosphere to store carbon.

We next determine how net forestation creates the pattern of fFire changes in Fig. 7a through cross-correlation analysis. We cross-correlate multi-model mean annual zonal mean differences of fFire, land cover change variables, and climate variables related to fire weather (T_s and surface relative humidity RH_s; Fig. 7c). Changes in fFire are positively correlated with changes in grass fraction for all five models. Additionally, these
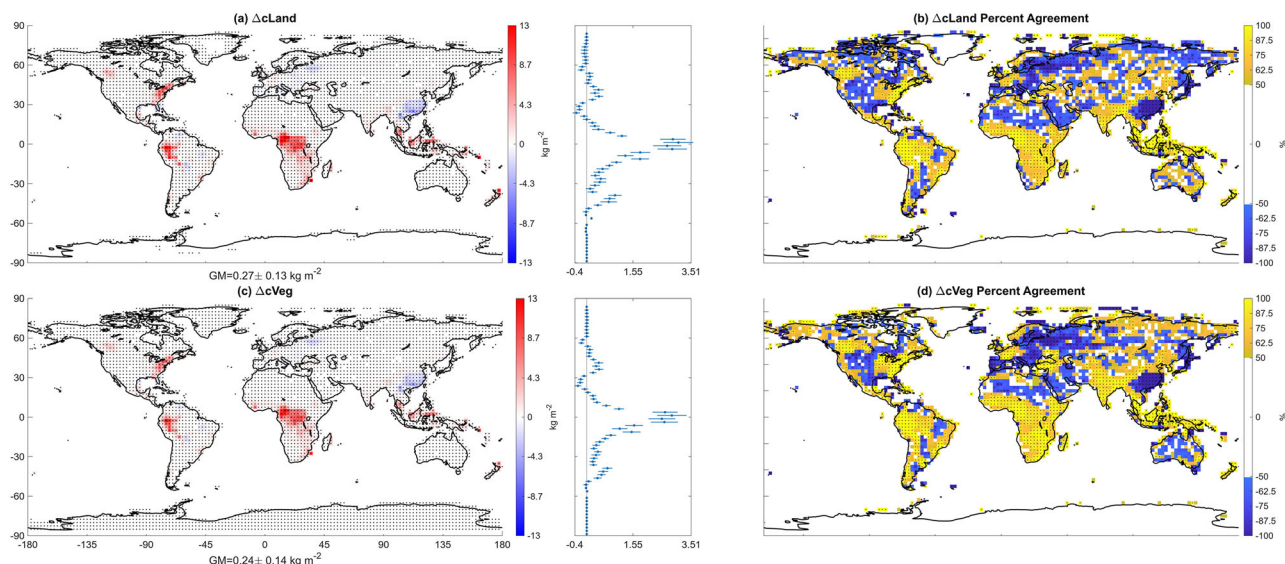
Fig. 5 | The biogeochemical effect of net forestation (ssp370-ssp126Lu − ssp370) over years 2070–2099. a, c depict the multi-model annual mean change in carbon stored in the land (cLand) and in the vegetation (cVeg), respectively (units are kg m^{-2}). The global mean change and its uncertainty are indicated underneath each panel. Black dots in (**a, c**) symbolize statistically significant differences at the 95% confidence interval using a two-tailed test. Depicted to the right of each multi-model mean map is a zonal mean of each variable, with the uncertainty based on the 95% confidence interval of the model spread. These plots share the same units as the color bar of the corresponding panel. The model percent agreement on the sign of these changes (%) is shown in (**b**) and (**d**) for $\Delta cLand$ and $\Delta cVeg$, respectively. Black dots in (**b, d**) symbolize 66% model agreement on the sign of the change.
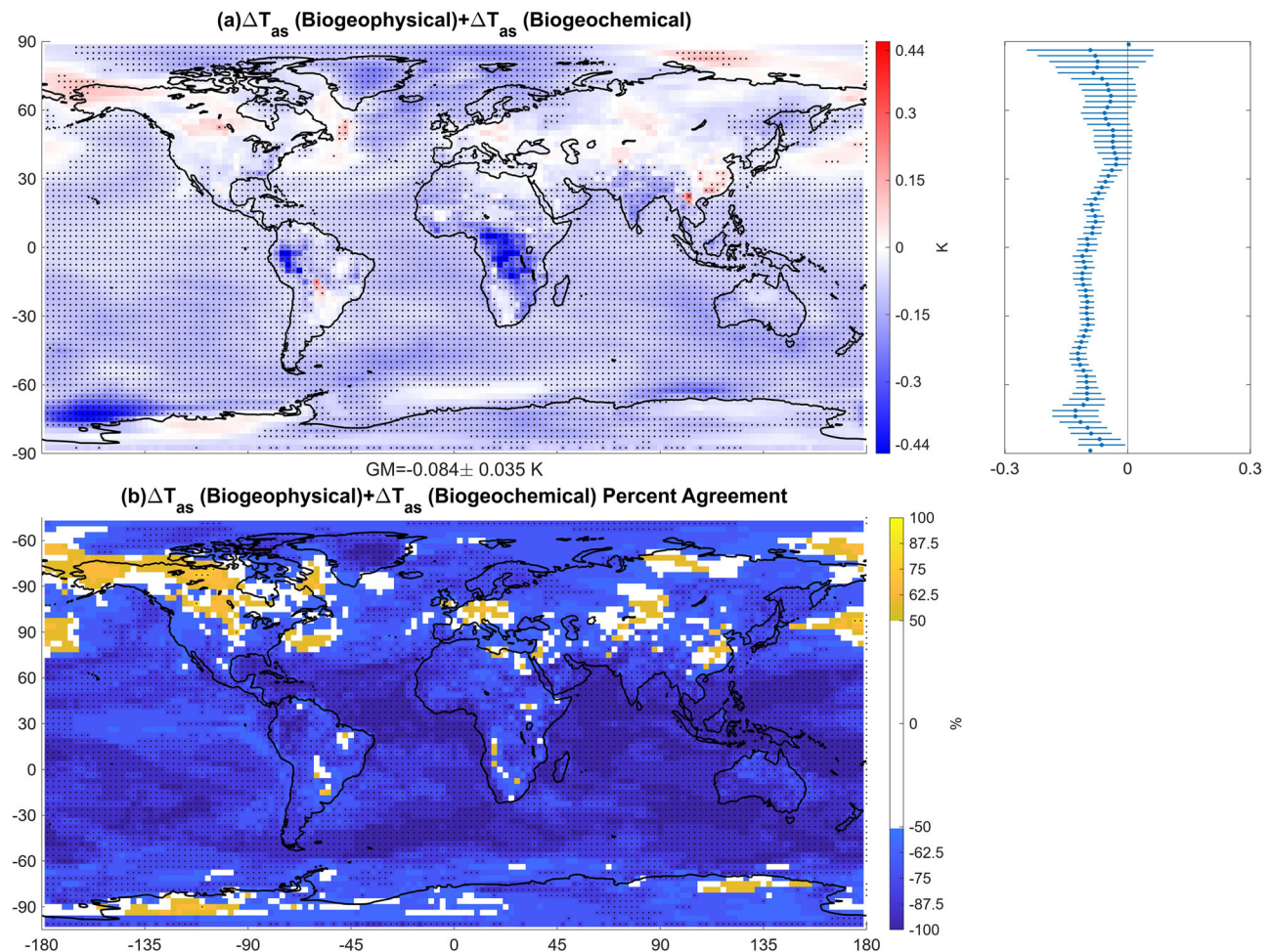
Fig. 6 | Biogeophysical plus TCRE-estimated biogeochemical effects of net forestation (ssp370-ssp126Lu − ssp370) over years 2070–2099. Multi-model annual mean response of (**a**) near-surface air temperature (T_{as}; K). Black dots symbolize statistically significant differences at the 95% confidence interval using a two-tailed test. The global mean change and its uncertainty are indicated underneath the panel. Depicted to the right is the corresponding zonal mean, with the uncertainty based on the 95% confidence interval of the model spread (units are K). Also shown is the model percent agreement plot (%) for (**b**) biogeophysical plus biogeochemical change in T_{as}. Yellow colors indicate that the majority of the models yield a positive difference. In contrast, blue colors indicate that the majority of the models yield a negative difference. Black dots on (**b**) show grid cells with at least 66% model agreement on the sign of the difference.

correlations are significant at the 95% confidence interval according to a two-tailed test for all five models. Four of the five models are also associated with negative correlations between *fFire* and tree fraction, with three models having significant negative correlations at the 95% confidence interval. Similarly, crop fraction and *fFire* have negative correlations for all five models, though only three are significant. Changes in climate variables, including T_s and RH_s, have much weaker correlations with the change in *fFire*, with only RH_s having a significant relationship with *fFire* at the 90% confidence interval. Therefore, this cross-correlation analysis suggests that changes in *fFire* under net forestation are primarily driven by the land cover change and not by the changes in climate due to the biogeophysical effects of net forestation. More specifically, increases in grass cover in these simulations (which are likely a result of crop abandonment as grass is the natural land cover in the region[54]) are associated with an increase in carbon fire emissions (e.g., GFDL-ESM4; Fig. 7c, Supplement Figs. S3f & S22c). Models with more decreases in grass fraction in the tropics (e.g., CESM2) have also decreased fire emissions (Fig. 7c, Supplement Figs. S3c & S22a). In contrast, increased cropland and tropical forests in these simulations are associated with decreased *fFire*.

Discussion

Our results suggest that net forestation, as specified by the difference between ssp370-ssp126Lu and ssp370, would help mitigate anthropogenically

induced global warming. The increase in land carbon storage produces an estimated global biogeochemical cooling of -0.08 ± 0.02 K. There is no significant global biogeophysical warming (rather, an insignificant cooling of -0.002 ± 0.04 K) associated with net forestation.

Regionally, there are differences in the net biogeophysical surface temperature response to net forestation. This includes general cooling of the tropics but warming of the northern hemisphere extratropics. While there is robust model agreement and significant multi-model mean albedo warming effects associated with forestation in mid-latitude regions, the latent cooling resulting from increased evapotranspiration in these areas is less certain. In contrast, relatively large and significant increases in evapotranspiration occur in the tropics, which dominate over the albedo effect locally. Tropical areas are associated with higher soil moisture, higher stomatal conductance, a lack of a winter dormancy period for tropical vegetation, and generally warmer overall temperatures; all these factors may lead to higher transpiration responses there[55-58]. Therefore, the higher efficiency of ET in the tropics compared to the mid-latitudes, as seen in Fig. 3c, is expected.

The lack of significant biogeophysical warming of net forestation is in contrast to prior studies that indicate that the biogeophysical effects could offset the biogeochemical effects by up to 50%[4-9]. This difference is partly related to the spatial location (and magnitude) of the land cover change examined here. For example, the land cover changes analyzed here show relatively small increases in temperate and particularly boreal trees, both of
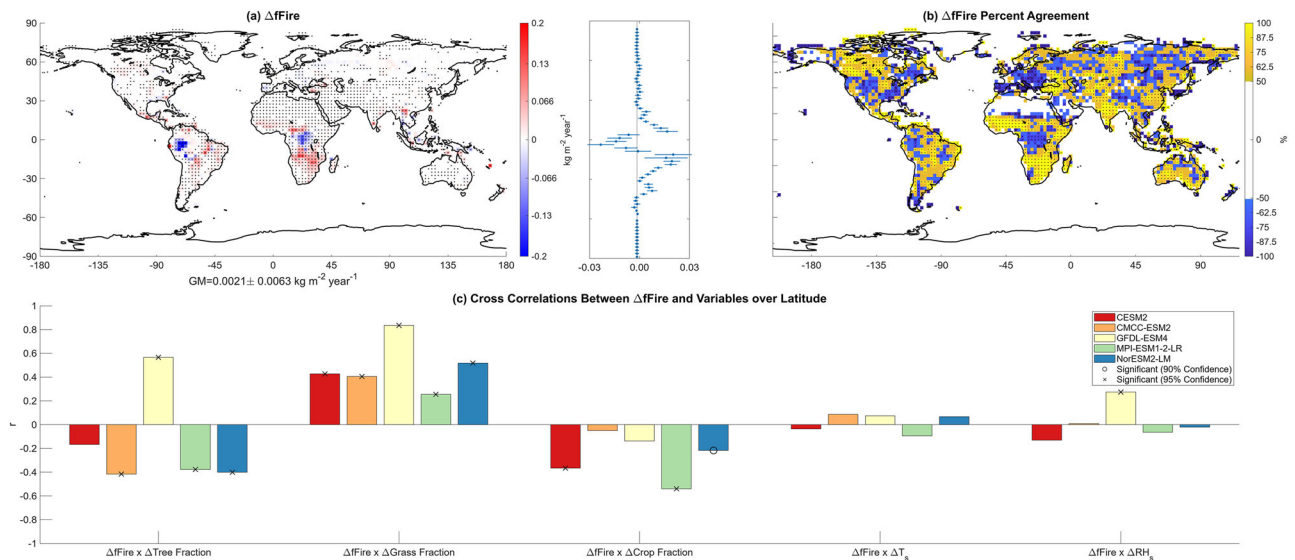
Fig. 7 | Change in fire carbon emissions under net forestation (ssp370-ssp126Lu − ssp370) over years 2070–2099. Multi-model annual mean response of (**a**) fire carbon emissions (*fFire*; kg m^{-2} year^{-1}). The global mean change and uncertainty are indicated underneath panel (**a**). Black dots in (**a**) symbolize statistically significant differences at the 95% confidence interval using a two-tailed test. Depicted to the right of (**a**) is a zonal mean of *fFire*, with the uncertainty based on the 95% confidence interval of the model spread. **b** Model percent agreement on the sign of the *fFire* response (%). Black dots in (**b**) symbolize 66% model agreement on the sign of the change. Also shown are (**c**) Pearson cross-correlation coefficients (*r*) between Δ*fFire* and tree fraction (Δ*treeFrac*), grass fraction (Δ*grassFrac*), crop fraction (Δ*cropFrac*), surface temperature (Δ*Ts*), and surface relative humidity (Δ*RHs*). Correlations are based on each variable's annual mean zonal mean land responses. ∘ symbolizes significant correlations at the 90% confidence interval and × symbolizes significant correlations at the 95% confidence interval according to a two-tailed test.

which are associated with a relatively large surface darkening (warming) biogeophysical effect. Much of the net forestation examined here is tropical and concentrated in central Africa.

Concerning aerosols, net forestation corresponds to a higher aerosol burden regionally, as organic aerosol increases in some models due to the increase in tree fraction (consistent with an increase in biogenic volatile organic compounds in these models). This increase in aerosol burden may help cool some regions. However, conclusions on the effects of net forestation on aerosol burden (as well as methane and ozone) require more study, as only three models involved in this project have interactive atmospheric chemistry and interactive biogenic volatile organic compound emissions. Additionally, the aerosol response in some models may be due to increases in dust from an increase in bare soil fraction in northern Africa.

There are some significant changes in near-surface air temperature over the ocean that indicate remote climate effects under net forestation, potentially related to changes in atmospheric/ocean circulation (e.g., temperature advection from afforested areas). However, the lack of multiple realizations for most models means that these significant changes in ocean temperatures could be due to internal climate variability. Therefore, further work is needed to draw concrete conclusions on the topic.

The fire response under net forestation shows minimal negative impact on carbon sequestration. In central Africa, for example, there is a significant decrease in fire carbon emissions, which would enhance carbon storage in the biosphere there. One consequence of net forestation is increased fire carbon emissions outside of tropical forests, especially in western and southern Africa. However, this increase in fire carbon emissions is due to higher grass fraction from crop abandonment in western and southern Africa, as opposed to an increase in tree fraction. However, we note some significant regional increases in fire carbon emissions associated with an increase in trees in boreal North America. Furthermore, only five of the models analyzed have an interactive fire module for these experiments, and three have the same fire module[52,53]. Based on this lack of model diversity and the large uncertainty in the change in fire carbon emissions, caution is warranted with these results.

One caveat is that the land cover change differs across some of the models, contributing to the inter-model uncertainty in the climate response. This is because some models have different ways of implementing the land cover change. This could be due to whether or not the model uses a dynamic global vegetation model or how the models implement the common harmonized land use drivers[46]. For example, although CESM2, CMCC-ESM2, and NorESM2-LM all share the same land cover change, including widespread forestation at the expense of grass in tropical Africa, CanESM5 (which has no dynamic vegetation) and GFDL-ESM4 (which has dynamic vegetation) have much weaker forestation there and even have increases in grass (Supplement Figs. S2 & S3). Models with a larger increase in tree fraction in this region generally have more significant cooling there. Similar statements apply to the mid-latitudes, where some models show forestation in western Europe, while other models show deforestation. There are also noticeable differences in the forestation effect on albedo and latent heat fluxes among models (e.g., that may stem from differences in stomatal conductance, plant hydraulics, parameters related to surface and vegetation albedo, etc). For example, models that experience net global warming yield weaker latent cooling at the equator and more albedo-driven warming in the northern hemisphere. Therefore, further understanding of the causes of these differences among the models is needed.

Despite these limitations, the CMIP6 multi-model ensemble mean analyzed in this paper shows no significant warming effect from the biogeophysical impacts of net forestation and relatively modest cooling associated with the biogeochemical effect. Aside from a significant increase in fire activity just outside the tropics, these simulations show few significant climate-specific drawbacks to supplementing traditional CO_2 mitigation techniques with forestation at low latitudes. Therefore, this study indicates that forestation, tree preservation, and reforestation of the tropics (15°S-15°N latitude) would reduce global CO_2 concentrations, have latent cooling effects, and may decrease fire carbon emissions in some tropical regions (e.g., central Africa). However, caution should be taken regarding forestation efforts elsewhere. Additionally, given the relatively weak cooling effects under the land cover change examined here, emissions reductions remain the dominant lever to address anthropogenically induced climate change.

Methods

CMIP6 models and experiments

We analyze output from 12 CMIP6 Earth System Models (Supplementary Table S1). Our analysis examines the difference between a global mean forestation experiment (ssp370-ssp126Lu) and a global mean deforestation experiment (ssp370), which we refer to as "net forestation" (Supplement Fig. S1). We emphasize that the difference between the scenarios represents a change in which afforestation, reforestation, and avoided deforestation contribute to "net" forestation, so this is an imperfect test case for constraining the impact of forestation on regional and global climate.

The ssp370 experiment is driven by a variant of the SSP3 "regional rivalry" IPCC scenario. It represents a future with medium-to-low CO_2 emissions mitigation[42]. In the ssp370 experiment, there is high deforestation to make room for more crops to feed a growing population and to support a higher gross domestic product. The ssp370-ssp126Lu experiment is the same as the ssp370 experiment concerning anthropogenic activity (e.g., atmospheric CO_2 and other greenhouse gas concentrations, aerosol emissions, etc.) and all other factors, excluding land use and land cover. In particular, ssp370-ssp126Lu uses land cover from the SSP1-2.6 scenario as opposed to that based on the SSP3-7.0 scenario. As such, ssp370-ssp126Lu replaces much cropland and grassland in the ssp370 experiment with trees (Fig. 2, Supplement Figs. S1–S4) and avoids most deforestation in the ssp370 experiment. However, there are a few notable exceptions. For example, the difference between scenarios leads to net deforestation in China (and parts of eastern Europe) and net crop fraction increase in the Sahel at the expense of bare soil (Supplement Figs. S1, S2, S4, & S6). The land use and land cover in each scenario are determined by an Integrated Assessment Model (IAM), which determines how land cover evolves through the 21st Century based on policy decisions and socioeconomic factors[42,47].

Within the 12 CMIP6 models, the land and atmosphere (and ocean and sea-ice) models are coupled. Therefore, there is two-way feedback between the land and the atmosphere that allows direct quantification of the biogeophysical effects. However, the simulations have no land (or ocean) carbon feedbacks onto the atmosphere (i.e., simulations use prescribed atmospheric CO_2 concentrations and are not driven by CO_2 emissions). As such, the impact of carbon storage in vegetation and soil does not influence atmospheric CO_2 concentration and air temperature; rather, the impact of the biogeochemical effects on air temperature is estimated offline using the TCRE. While three of the models (CESM, NorESM2, CMCC) share variations of the same land model and thus the same land cover change (e.g., models that utilize CLM4.5 or CLM5; Supplement Figs. S2–S4), other models have slightly different land cover changes. Some employ dynamic vegetation models that project vegetation cover, overriding the prescribed land cover except where the transition to or from crop area is concerned (Supplement Figs. S2–S6).

The experiments begin in 2015 and are run for 85 years, except for the NorESM2-LM ssp370-ssp126Lu experiment, which ends in 2099 instead of 2100. Therefore, 2099 is taken as the last year for each experiment and model. For this analysis, the years 2070–2099 (the last 30 years) are averaged together for each experiment and model. The 30-year average for the global mean deforestation experiment (ssp370) is then subtracted from the global mean forestation experiment (ssp370-ssp126Lu) to obtain the effect of the land cover change. Previous studies have compared these two experiments to analyze future changes in temperature and precipitation extremes[44,45]. However, these studies did not investigate mechanisms driving these extremes or quantify general regional or global mean changes in important parameters such as fire. A list and description of the variable abbreviations used within this paper and the corresponding CMIP6 variable from which it is derived can be found in Supplement Table S4.

Dynamic vegetation models

Most of the ESMs used here do not employ a Dynamic Global Vegetation Model (DGVM) and thus do not simulate changes in the distribution and type of vegetation in response to changes in CO_2, climate, fire, or vegetation competition. However, all models simulate changes in vegetation physiology and state, such as leaf area index and canopy height[27,59].

Three models include a DGVM, including UKESM1-0-LL, MPI-ESM1-2-LR, and GFDL-ESM4, and thus simulate changes in the type of vegetation, also known as plant functional types (PFTs). More information on DGVMs can be found in supplement section 2.

Fire modules

Of the models used in this analysis, five have fire modules with output in the CMIP6 archive for the ssp370-ssp126Lu experiment (Supplement Table S2). Taking the difference between the ssp370-ssp126Lu experiment and the ssp370 experiment yields the response of fire carbon emissions to the effects of the land cover change and its biogeophysical effects. As the atmospheric CO_2 concentration between the two experiments is the same, there are no temperature-related biogeochemical effects on fire occurrence (or climate). However, there are effects on CO_2 fertilization due to the differences in land cover type (trees respond differently to higher CO_2 concentration than other vegetation types[27]). We also note that human ignitions and suppression of fires are identical between both ssp370 and ssp370-ssp126Lu as both processes are parameterized based on the human population, which evolves identically in both experiments. Furthermore, none of the models in the experiments employ interactive fire emissions of trace gases and aerosols; instead, they employ prescribed fire emissions of trace gases and aerosols, which thus have a mismatch with interactive carbon emissions and impacts. As aerosols emitted from fires can have shortwave and longwave effects that significantly alter the climate (e.g.,[27,60]), the climate impacts of fires in this experimental design are not completely captured as biomass burning aerosols are the same between both simulations. More information on how fire modules operate and the uncertainty associated with them can be found in supplement section 3.

Representation of atmospheric chemistry and composition

Emissions of anthropogenic and biomass burning trace gases, aerosols, and precursors are prescribed by SSP370 in both ssp370 and ssp370-ssp126Lu experiments. Only three of the models include interactive chemistry (GFDL-ESM4, NorESM2-LM, and UKESM1-0-LL)[23,61–63], which includes interactive BVOC emissions and their effects on atmospheric constituents such as secondary organic aerosol (SOA) and ozone (but not methane). In models with interactive BVOC emissions, the emissions respond to climate change (e.g., changes in CO_2, temperature, etc.) and, in most cases, vegetation change too. In GFDL-ESM4, however, the vegetation model is decoupled from the BVOC module, and therefore, the BVOC emissions only respond to changes in climate. NorESM2-LM and GFDL-ESM4 simulate BVOC emissions using the Model of Emissions of Gases and Aerosols from Nature (MEGAN[64]). MEGAN BVOC emissions are based on a variety of factors, including sunlight[65], a temperature response based on enzymatic activity[65], and a CO_2 response based on changes in metabolite pools, enzyme activity, and gene expression[66]. Different models have different implementations of the factors and number of factors included. For example, GFDL-ESM4 does not include CO_2-isoprene inhibition.

All of the models used have interactive dust emission schemes. Dust emission is generally a function of leaf area index, bare soil fraction, soil moisture, and/or wind speed, though the exact formulation depends on the model (Supplement Table S2).

Surface energy balance decomposition

We utilize the surface energy balance decomposition (SEBD) method to estimate the contribution of changes in surface energy fluxes to changes in surface temperature[5]. The SEBD assumes that the change in T_s is directly related to the change in surface radiative fluxes and the surface sensible and latent heat fluxes. However, the SEBD does not consider every aspect of surface energy transfer (such as sub-surface heat exchange) and may inaccurately simulate T_s in some areas. We only apply the SEBD to areas with an increase or decrease in the tree fraction of 1% or greater to understand the drivers of the surface temperature response directly due to the tree fraction change.

In comparing an experiment to a control (i.e., ssp370-ssp126Lu versus ssp370), surface temperature response can be approximated as

$$\Delta T_s = \frac{1}{4\epsilon\sigma T_{s,control}^3}(\Delta SW_d(1-\alpha) - \Delta\alpha(SW_d) + \Delta LW_d - \Delta LE - \Delta H) \quad (1)$$

where ΔT_s is the change in surface temperature for the ssp370-ssp126Lu experiment compared to the ssp370 experiment, $T_{s,control}$ is the surface temperature of the ssp370 experiment, ϵ is the surface emissivity (approximated to be 0.97)[67], and σ is the Stefan-Boltzmann constant (with a value of 5.67×10^{-8} W m^{-2} K^{-4}). The first term in parentheses represents the contribution from changes in surface downwelling shortwave radiation (ΔSW_d); the second term represents the contribution from changes in surface albedo ($\Delta\alpha$); the third term represents the contribution from changes in surface downwelling longwave radiation (ΔLW_d); the fourth term represents the contribution from changes in surface latent heat flux (ΔLE); and the fifth term represents the contribution from changes in surface sensible heat flux (ΔH).

Transient climate response to cumulative CO$_2$ Emissions
The change in carbon stored in land ($\Delta cLand$) due to net forestation is given by

$$\Delta cLand = \Delta cVeg + \Delta cSoil + \Delta cLitter \quad (2)$$

where $\Delta cSoil$ is the carbon stored in soil organic matter and $cLitter$ is the carbon stored in litter. With the $\Delta cLand$ value, the biogeochemical effect of net forestation on global mean T_{as} is given by

$$\Delta T_{as} = \Delta TCRE \times \Delta cLand \quad (3)$$

where $\Delta TCRE$ represents a near-linear relationship between cumulative anthropogenic CO$_2$ emissions and global warming since the preindustrial and provides a good first estimate of the near-surface air temperature response to land carbon changes. The values of $TCRE$ used for each model are given by ref. 68 and displayed in Supplement Table S3. For the CMCC-ESM2 model, a value of 1.77 K per 1 EgC is used based on the multi-model average $TCRE$ in ref. 68.

Data processing and statistics
The data processing and statistics utilized in this paper follow the methods of refs. 23,27. Using bilinear interpolation, we utilize monthly mean CMIP6 data and spatially re-grid all model data to a 2.5° × 2.5° grid. We calculate the net forestation response as the difference in years 2070-2099 from ssp370-ssp126Lu relative to the same years from the ssp370 simulation. The multi-model mean is estimated from the average of all the models. If multiple ensemble members are available for a given model, we first (i.e., before calculating the multi-model average) calculate an ensemble average of that model.

We emphasize the limitations of our study in terms of the lack of availability of multiple ensemble members for each model. We use one ensemble member for most models, as only one realization is available for these experiments. Multiple realizations are available for ACCESS-ESM1-5, UKESM1-0-LL, and CESM2, and we use 10, 5, and 3 realizations, respectively (Supplement Table S1). For the models with multiple realizations, we examine the ensemble average T_{as} and agreement in Supplement Fig. S23. We generally find robust (2/3rds agreement on the sign of the change among realizations) in T_{as} for all models in areas with significant forest cover increase (e.g., Central Africa). However, in many areas where the forestation signal is weaker, there is less agreement on the sign of the change, highlighting a need for multiple ensemble members to discern robust responses.

Statistical significance of the climate response is calculated using two different methods. In the first method, which is illustrated via dots on maps (e.g., Fig. 3a), we calculate the multi-model mean time series for both the ssp370-ssp126Lu (experiment) and the ssp370 (control) simulations, and we then calculate the 2070–2099 difference between the two for a given

variable. We use a two-tailed paired t-test to assess significance, where the null hypothesis of a zero difference is evaluated at the 95% confidence interval, with n-1 degrees of freedom, n is the number of years in the experiment (30 years). Here, the paired variance,

$$\frac{1}{n-1}\sum_{i=1}^{n}(d_i - \bar{d})^2 \quad (4)$$

is used, where d_i is the difference between experiment and control for a given year, and $\bar{d}$ is the average difference between the experiment and control over all time. The paired t-test has been used extensively in past CMIP6 analyses[69–71].

We also determine the statistical significance of the multi-model mean response relative to the response of each model (the results of this testing are given in the text to quantify global and regional uncertainty as well as in the zonal averages). Here, we calculate the multi-model mean response as the average of the individual model responses, and its uncertainty is estimated as plus/minus 1.96 × standard error (i.e., the 95% confidence interval) according to

$$\frac{1.65 \times \sigma}{\sqrt{n_m}} \quad (5)$$

where σ is the standard deviation across models and n_m is the number of models. If this confidence interval does not include zero, then the multi-model mean response is significant at the 95% confidence level.

We also estimate the model agreement on the sign of the model-mean response (e.g., the yellow versus blue coloring on maps like Fig. 3b), which is determined at each grid cell as the percentage of models that have a positive or negative response. Grid cells for which 66% (i.e., 2/3) of the models agree on a sign pass a 2-tailed binomial test to reject the null hypothesis of equal probability of positive or negative sign at the 95% confidence level. Under such conditions, there is robust agreement on the sign of the response across the models (designated by symbols).

Concerning cross-correlation analysis, the statistical significance of the Pearson cross-correlation coefficient (r) is approximated from a two-tailed t-test as:

$$t = \frac{r}{\sqrt{\frac{1-r^2}{N-2}}} \quad (6)$$

with N-2 degrees of freedom. For correlations performed over latitude, N is the length of a variable's latitude dimension (with missing values removed), as the correlations are performed zonally. For correlations performed on a grid cell-by-grid cell basis, N is the total number of grid cells used in the calculation. For correlations performed across models, N is the number of models. Cross correlations are deemed significant if the p-value is under 0.1 (i.e., the 90% confidence interval).

Data availability
CMIP6 data can be downloaded from the Earth System Grid Federation at https://esgf-node.llnl.gov/search/cmip6/. Standard code was used to analyze CMIP6 data, which is available upon request from jgome222@ucr.edu.

References
1. Nilsson, S. & Schopfhauser, W. The carbon-sequestration potential of a global afforestation program. *Climatic Change* **30**, 267–293 (1995).
2. Doelman, J. C. et al. Afforestation for climate change mitigation: Potentials, risks and trade-offs. *Glob. Change Biol.* **26**, 1576–1591 (2020).
3. Ito, A. et al. Soil carbon sequestration simulated in CMIP6-LUMIP models: implications for climatic mitigation. *Environ. Res. Lett.* **15**, 124061 (2020).

4. Anderson, R. G. et al. Biophysical considerations in forestry for climate protection. *Front. Ecol. Environ.* **9**, 174–182 (2011).

5. Boysen, L. R. et al. Global climate response to idealized deforestation in CMIP6 models. *Biogeosciences* **17**, 5615–5638 (2020).

6. Weber, J. et al. Chemistry-albedo feedbacks offset up to a third of forestation's CO2 removal benefits. *Science* **383**, 860–864 (2024).

7. Jayakrishnan, K. U. & Bala, G. A comparison of the climate and carbon cycle effects of carbon removal by afforestation and an equivalent reduction in fossil fuel emissions. *Biogeosciences* **20**, 1863–1877 (2023).

8. Wang, Y., Yan, X. & Wang, Z. Global warming caused by afforestation in the Southern Hemisphere. *Ecol. Indic.* **52**, 371–378 (2015).

9. Betts, R. A. Offset of the potential carbon sink from boreal forestation by decreases in surface albedo. *Nature* **408**, 187–190 (2000).

10. Luyssaert, S. et al. Land management and land-cover change have impacts of similar magnitude on surface temperature. *Nat. Clim. Change* **4**, 389–393 (2014).

11. Tang, T. et al. Biophysical Impact of Land-Use and Land-Cover Change on Subgrid Temperature in CMIP6 Models. *J. Hydrometeorol.* **24**, 373–388 (2023).

12. Obregón, M. A., Costa, M. J., Silva, A. M. & Serrano, A. Impact of aerosol and water vapour on SW radiation at the surface: Sensitivity study and applications. *Atmos. Res.* **213**, 252–263 (2018).

13. Scott, C. E. et al. Substantial large-scale feedbacks between natural aerosols and climate. *Nat. Geosci.* **11**, 44–48 (2018).

14. Thornhill, G. et al. Climate-driven chemistry and aerosol feedbacks in CMIP6 Earth system models. *Atmos. Chem. Phys.* **21**, 1105–1126 (2021).

15. Scott, C. E. et al. Impact on short-lived climate forcers increases projected warming due to deforestation. *Nat. Commun.* **9**, 157 (2018).

16. Unger, N. Human land-use-driven reduction of forest volatiles cools global climate. *Nat. Clim. Change* **4**, 907–910 (2014).

17. Rohatyn, S., Rotenberg, E., Tatarinov, F., Carmel, Y. & Yakir, D. Large variations in afforestation-related climate cooling and warming effects across short distances. *Commun. Earth Environ.* **4**, 1–10 (2023).

18. Arora, V. K. & Montenegro, A. Small temperature benefits provided by realistic afforestation efforts. *Nat. Geosci.* **4**, 514–518 (2011).

19. Peng, S.-S. et al. Afforestation in China cools local land surface temperature. *Proc. Natl. Acad. Sci.* **111**, 2915–2919 (2014).

20. Bhattarai, H., Tai, A. P. K., Val Martin, M. & Yung, D. H. Y. Impacts of changes in climate, land use, and emissions on global ozone air quality by mid-21st century following selected Shared Socioeconomic Pathways. *Sci. Total Environ.* **906**, 167759 (2024).

21. Evans, S., Ginoux, P., Malyshev, S. & Shevliakova, E. Climate-vegetation interaction and amplification of Australian dust variability. *Geophys. Res. Lett.* **43**, 11,823–11,830 (2016).

22. Zhao, A., Ryder, C. L. & Wilcox, L. J. How well do the CMIP6 models simulate dust aerosols? *Atmos. Chem. Phys.* **22**, 2095–2119 (2022).

23. Gomez, J. et al. The projected future degradation in air quality is caused by more abundant natural aerosols in a warmer world. *Commun. Earth Environ.* **4**, 1–11 (2023).

24. Laguë, M. M. & Swann, A. L. S. Progressive Midlatitude Afforestation: Impacts on Clouds, Global Energy Transport, and Precipitation. *J. Clim.* **29**, 5561–5573 (2016).

25. Portmann, R. et al. Global forestation and deforestation affect remote climate via adjusted atmosphere and ocean circulation. *Nat. Commun.* **13**, 5569 (2022).

26. Barnes, M. L. et al. A Century of Reforestation Reduced Anthropogenic Warming in the Eastern United States. *Earth's. Future* **12**, e2023EF003663 (2024).

27. Allen, R. J., Gomez, J., Horowitz, L. W. & Shevliakova, E. Enhanced future vegetation growth with elevated carbon dioxide concentrations could increase fire activity. *Commun. Earth Environ.* **5**, 1–15 (2024).

28. Nunes, J. P. et al. Afforestation, Subsequent Forest Fires and Provision of Hydrological Services: A Model-Based Analysis for a Mediterranean Mountainous Catchment. *Land Degrad. Dev.* **29**, 776–788 (2018).

29. Goforth, B. R. & Minnich, R. A. Densification, stand-replacement wildfire, and extirpation of mixed conifer forest in Cuyamaca Rancho State Park, southern California. *For. Ecol. Manag.* **256**, 36–45 (2008).

30. Jones, M. W. et al. Global and Regional Trends and Drivers of Fire Under Climate Change. *Rev. Geophys.* **60**, e2020RG000726 (2022).

31. Kukavskaya, E. A., Shvetsov, E. G., Buryak, L. V., Tretyakov, P. D. & Groisman, P. Y. Increasing Fuel Loads, Fire Hazard, and Carbon Emissions from Fires in Central Siberia. *Fire* **6**, 63 (2023).

32. van Wees, D. et al. Global biomass burning fuel consumption and emissions at 500 m spatial resolution based on the Global Fire Emissions Database (GFED). *Geoscientific Model Dev.* **15**, 8411–8437 (2022).

33. DellaSala, D. A., Baker, B. C., Hanson, C. T., Ruediger, L. & Baker, W. Have western USA fire suppression and megafire active management approaches become a contemporary Sisyphus? *Biol. Conserv.* **268**, 109499 (2022).

34. Gaboriau, D. M. et al. Temperature and fuel availability control fire size/severity in the boreal forest of central Northwest Territories, Canada. *Quat. Sci. Rev.* **250**, 106697 (2020).

35. Walker, X. J. et al. Fuel availability not fire weather controls boreal wildfire severity and carbon emissions. *Nat. Clim. Change* **10**, 1130–1136 (2020).

36. Parisien, M.-A. et al. Fire deficit increases wildfire risk for many communities in the Canadian boreal forest. *Nat. Commun.* **11**, 2121 (2020).

37. Dodge, M. Forest Fuel Accumulation-A Growing Problem. *Science* **177**, 139–142 (1972).

38. Jolly, W. M. et al. Climate-induced variations in global wildfire danger from 1979 to 2013. *Nat. Commun.* **6**, 7537 (2015).

39. Abatzoglou, J. T., Williams, A. P. & Barbero, R. Global Emergence of Anthropogenic Climate Change in Fire Weather Indices. *Geophys. Res. Lett.* **46**, 326–336 (2019).

40. Ruffault, J. et al. Increased likelihood of heat-induced large wildfires in the Mediterranean Basin. *Sci. Rep.* **10**, 13790 (2020).

41. Richardson, D. et al. Global increase in wildfire potential from compound fire weather and drought. *npj Clim. Atmos. Sci.* **5**, 1–12 (2022).

42. O'Neill, B. C. et al. The Scenario Model Intercomparison Project (ScenarioMIP) for CMIP6. *Geoscientific Model Dev.* **9**, 3461–3482 (2016).

43. Lawrence, D. M. et al. The Land Use Model Intercomparison Project (LUMIP) contribution to CMIP6: rationale and experimental design. *Geoscientific Model Dev.* **9**, 2973–2998 (2016).

44. Hong, T., Wu, J., Kang, X., Yuan, M. & Duan, L. Impacts of Different Land Use Scenarios on Future Global and Regional Climate Extremes. *Atmosphere* **13**, 995 (2022).

45. Zhang, M., Gao, Y., Zhang, L. & Yang, K. Impacts of anthropogenic land use and land cover change on climate extremes based on CMIP6-LUMIP experiments: part II. Future period. *Clim. Dyn.* **62**, 3669–3688 (2024).

46. Chini, L. et al. Land-use harmonization datasets for annual global carbon budgets. *Earth Syst. Sci. Data* **13**, 4175–4189 (2021).

47. Shiogama, H. et al. Important distinctiveness of SSP3-7.0 for use in impact assessments. *Nat. Clim. Change* **13**, 1276–1278 (2023).

48. Winckler, J. et al. Different response of surface temperature and air temperature to deforestation in climate models. *Earth Syst. Dyn.* **10**, 473–484 (2019).

49. Li, Y. et al. Observed different impacts of potential tree restoration on local surface and air temperature. *Nat. Commun.* **16**, 2335 (2025).

50. Vargas Zeppetello, L. R., Donohoe, A. & Battisti, D. S. Does Surface Temperature Respond to or Determine Downwelling Longwave Radiation? *Geophys. Res. Lett.* **46**, 2781–2789 (2019).

51. Meehl, G. A. et al. Context for interpreting equilibrium climate sensitivity and transient climate response from the CMIP6 Earth system models. *Sci. Adv.* **6**, eaba1981 (2020).

52. Li, F., Zeng, X. D. & Levis, S. A process-based fire parameterization of intermediate complexity in a Dynamic Global Vegetation Model. *Biogeosciences* **9**, 2761–2780 (2012).

53. Li, F. et al. Historical (1700-2012) global multi-model estimates of the fire emissions from the Fire Modeling Intercomparison Project (FireMIP). *Atmos. Chem. Phys.* **19**, 12545–12567 (2019).

54. Loughran, T. F. et al. Limited Mitigation Potential of Forestation Under a High Emissions Scenario: Results From Multi-Model and Single Model Ensembles. *J. Geophys. Res.: Biogeosci.* **128**, e2023JG007605 (2023).

55. Zhou, S., Zhang, Y., Park Williams, A. & Gentine, P. Projected increases in intensity, frequency, and terrestrial carbon costs of compound drought and aridity events. *Sci. Adv.* **5**, eaau5740 (2019).

56. Nemani, R. R. et al. Climate-Driven Increases in Global Terrestrial Net Primary Production from 1982 to 1999. *Science* **300**, 1560–1563 (2003).

57. Yuan, W. et al. Increased atmospheric vapor pressure deficit reduces global vegetation growth. *Sci. Adv.* **5**, eaax1396 (2019).

58. Wang, R. et al. Latitudinal variation of leaf stomatal traits from species to community level in forests: linkage with ecosystem productivity. *Sci. Rep.* **5**, 14454 (2015).

59. Rabin, S. S. et al. The Fire Modeling Intercomparison Project (FireMIP), phase 1: experimental and analytical protocols with detailed model descriptions. *Geoscientific Model Dev.* **10**, 1175–1197 (2017).

60. Gomez, J. L., Allen, R. J. & Li, K.-F. California wildfire smoke contributes to a positive atmospheric temperature anomaly over the western United States. *Atmos. Chem. Phys.* **24**, 6937–6963 (2024).

61. Horowitz, L. W. et al. The GFDL Global Atmospheric Chemistry-Climate Model AM4.1: Model Description and Simulation Characteristics. *J. Adv. Modeling Earth Syst.* **12**, e2019MS002032 (2020).

62. Kirkevåg, A. et al. A production-tagged aerosol module for Earth system models, OsloAero5.3 - extensions and updates for CAM5.3-Oslo. *Geoscientific Model Dev.* **11**, 3945–3982 (2018).

63. Archibald, A. T. et al. Description and evaluation of the UKCA stratosphere-troposphere chemistry scheme (StratTrop vn 1.0) implemented in UKESM1. *Geoscientific Model Dev.* **13**, 1223–1266 (2020).

64. Guenther, A. B. et al. The Model of Emissions of Gases and Aerosols from Nature version 2.1 (MEGAN2.1): an extended and updated framework for modeling biogenic emissions. *Geoscientific Model Dev.* **5**, 1471–1492 (2012).

65. Guenther, A. B., Monson, R. K. & Fall, R. Isoprene and monoterpene emission rate variability: Observations with eucalyptus and emission rate algorithm development. *J. Geophys. Res.: Atmospheres* **96**, 10799–10808 (1991).

66. Wilkinson, M. J. et al. Leaf isoprene emission rate as a function of atmospheric CO2 concentration. *Glob. Change Biol.* **15**, 1189–1200 (2009).

67. Hirsch, A. L. et al. Modelled biophysical impacts of conservation agriculture on local climates. *Glob. Change Biol.* **24**, 4758–4774 (2018).

68. Arora, V. K. et al. Carbon-concentration and carbon-climate feedbacks in CMIP6 models and their comparison to CMIP5 models. *Biogeosciences* **17**, 4173–4222 (2020).

69. Zanis, P. et al. Fast responses on pre-industrial climate from present-day aerosols in a CMIP6 multi-model study. *Atmos. Chem. Phys.* **20**, 8381–8404 (2020).

70. Su, T., Li, Z. & Zheng, Y. Cloud-Surface Coupling Alters the Morning Transition From Stable to Unstable Boundary Layer. *Geophys. Res. Lett.* **50**, e2022GL102256 (2023).

71. Wei, N. et al. Impact of precipitation-induced sensible heat on the simulation of land-surface air temperature. *J. Adv. Modeling Earth Syst.* **6**, 1311–1320 (2014).

Acknowledgements

Author contributions

J.L.G. performed data analysis, prepared all figures, designed the study, and wrote the paper. R.J.A. conceived the project, designed the study, and wrote the paper. S.T.T. performed UKESM1-0-LL simulations and provided additional data. L.W.H. performed GFDL-ESM4 simulations and provided additional data. R.A.F. advised on methods. All authors discussed results and contributed to the writing of the manuscript.

Competing interests

The authors declare no competing interests.

Additional information

Supplementary information The online version contains supplementary material available at https://doi.org/10.1038/s41612-025-01127-4.

Correspondence and requests for materials should be addressed to James L. Gomez.

Reprints and permissions information is available at http://www.nature.com/reprints

Publisher's note Springer Nature remains neutral with regard to jurisdictional claims in published maps and institutional affiliations.